We are IntechOpen, the world's leading publisher of Open Access books Built by scientists, for scientists

6,900
Open access books available

185,000
International authors and editors

200M
Downloads

Our authors are among the

154
Countries delivered to

TOP 1%
most cited scientists

12.2%
Contributors from top 500 universities



WEB OF SCIENCE™

Selection of our books indexed in the Book Citation Index in Web of Science™ Core Collection (BKCI)

Interested in publishing with us?
Contact book.department@intechopen.com

Numbers displayed above are based on latest data collected.
For more information visit www.intechopen.com



11

Determining Exact Point Correspondences in 3D Measurement Systems Using Fringe Projection – Concepts, Algorithms and Accuracy Determination

Christian Bräuer-Burchardt, Max Möller, Christoph Munkelt,
Matthias Heinze, Peter Kühmstedt and Gunther Notni
Fraunhofer IOF Jena, Jena,
Germany

1. Introduction

Fringe projection systems for contactless surface measurements are increasingly used in applications of industrial inspection, quality control, rapid prototyping, archaeology, and in medical applications. Such systems provide increasing accuracy together with shorter measurement time and increasing data volume. The demands of increasing data volume, accuracy, and measurement speed can be satisfied using a more powerful calculation technique and better algorithms.

Calculation of 3D surface points by fringe projection systems is typically based on triangulation known from photogrammetry. An extensive review gives e.g. Luhmann (Luhmann et al., 2006). This involves the task of finding homologous points describing points in different images depicting the same original measuring point. In fringe projection systems the finding of homologous points typically uses phase information (Creath, 1986) of the points. The phase value characterizes the origin of a projected ray in the projector image plane. The projector is geometrically considered as an inverse camera (Schreiber & Notni, 2000).

When an optical contactless 3D measurement system has to be designed or selected among different alternatives some different basics should be clear. It must be known which objects should be measured, how fast the measurement should run, and how accurate the measurement has to be. If these aspects are plain, the design or selection may start. As the calculation of the resulting 3D points on the object's surface is based on triangulation, the procedure of finding corresponding points is crucial. This procedure has mainly two aspects: uniqueness and precision of the localized position of the corresponding points. In this work the various methods to obtain unique point correspondences are not described in detail, but rather the second aspect (precision) should be dealt with. Uniqueness of point correspondences is obtained by phase unwrapping (Sansoni et al., 1999; Reich et al., 2000). This can be realized e.g. by the use of multiple spatial frequencies (Li et al., 2005), temporal phase unwrapping methods (Zhang et al., 1999), or use of Gray code sequences (Sansoni et al., 1999). Due to its unambiguousness, the usage of Gray code leads to robust results.

An extensive survey over coded structured light techniques to solve the correspondence problem which is the basis for 3D surface reconstruction is given by Battle (Battle et al., 1998).

Zhang and Yau suggest a real-time coordinate measurement (Zhang & Yau, 2006) where phase unwrapping is realized by determination and tracking of a marker. An interesting method for phase unwrapping using at least two cameras is presented by Ishiyama (Ishiyama et al., 2007a). There the number of possible correspondences is drastically reduced by back-propagation of the correspondence candidates into the image of the second camera. Ishiyama gives another suggestion (Ishiyama et al., 2007b) for 3D measurement using the invariance of cross-ratio of perspective projection. Young (Young et al., 2007) suggests the use of the limitation of the measuring volume in order to reduce the search area for corresponding points on the epipolar line to segments achieving a reduction of the projected binary code by careful placement of additional cameras (or additional measuring positions). Li (Li et al., 2009) uses this approach in combination with the multi-frequency technique in order to realize real-time 3D measurements.

We presented an algorithm (Bräuer-Burchardt, 2011a) describing how one can obtain unique point correspondences using geometric constraints. This algorithm works when certain conditions as restricted measurement volume depth hold.

A number of works were published from our working group concerning accuracy determination of phase values and phase value based measurements (Notni & Notni, 2003; Bräuer-Burchardt et al., 2010). These works show the importance of theoretical error estimation as well as the performance of experimental error analysis of fringe projection based 3D surface measurement systems.

Different arrangements of camera(s) and projector(s) in 3D measuring systems using fringe projection have been recently proposed (Maas, 1992; Ishiyama et al., 2007a). Arising methods are based on triangulation (Luhmann et al., 2006) between two or bundle adjustment between more than two viewpoints (sensor positions), or between two camera positions within one sensor position. The most common triangulation procedure to obtain 3D measurement data in fringe projection systems is between two cameras or one camera and one projector (Schreiber & Notni, 2000; Reich, 2000).

We consider the case of having one or two cameras and one projector in our sensor head. We distinguish three kinds of establishing correspondences using one sensor position. The first one is the simple observation of a phase value (Creath, 1986; Schreiber & Notni, 2000) at a certain camera coordinate. The corresponding point in the projector image is directly yielded by the observed phase value. This method is called CP mode (one camera and one projector are used for triangulation). Another method is to search for the observed phase value in the second camera image denoted by CC (two cameras are used for triangulation). The third one called VR mode (virtual raster) uses a virtual projection grid and finds the phase values of the grid points in the two camera images. This method corresponds to the technique described by Reich (Reich et al., 2000).

In this work these different methods are compared regarding measurement accuracy, handling, and sensitivity against image disturbances. The measuring principles are briefly presented and advantages and disadvantages are discussed.

A model describing the random error of the resulting 3D measurement data was developed and confirmed by the results of simulation experiments and real data measurements obtained by two different measuring devices. The results are analysed and discussed and an outlook to future work is given.

2. Situation and measuring principles

Recently several fringe projection systems for 3D surface determination for different measurement objects were developed at our institute (Kühmstedt et al., 2005; Munkelt et al., 2005; Kühmstedt et al., 2007; Kühmstedt et al. 2007b; Bräuer-Burchardt et al., 2011b). Some of them are shown in figs.1 and 2. They are based on the projection and observation of one or two 90° rotated fringe sequences consisting of sinusoidal fringe patterns (between 3 and 16 images) and optionally of a Gray code sequence (usually 5 to 7 images). From these sequences phase values are determined using a 3-, 4-, 6-, 8-, or 16-phase algorithm (Kühmstedt et al., 2007). Phase values are used together with the extrinsic and intrinsic parameters of the optical components to determine the 3D point coordinates of the reconstructed object surface.

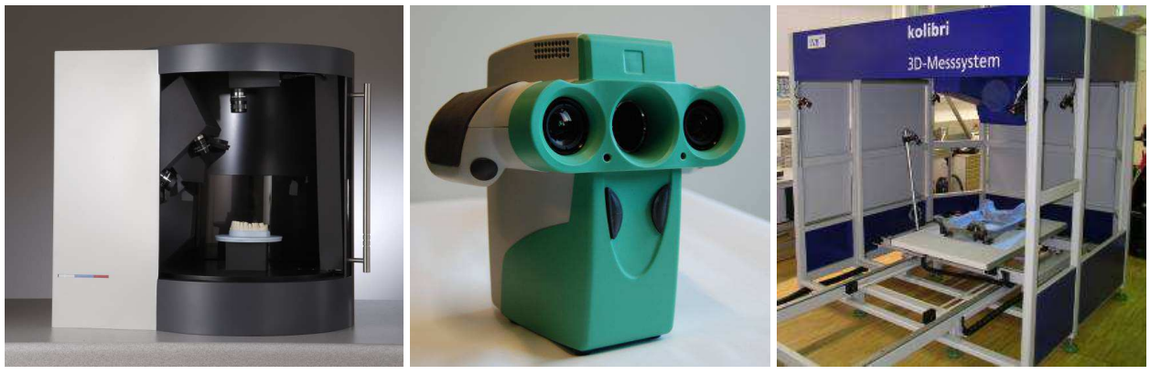


Fig. 1. Several fringe projection based measurement systems developed at Fraunhofer IOF: kolibri flex mini, kolibri CORDLESS, kolibri step (from left to right)

The use of epipolar constraint in order to find point correspondences is a typical approach in phototogrammetry (Luhmann et al., 2006). It reduces the task to a correspondence problem between two one-dimensional vectors.

Let us consider using a sensor consisting of two cameras C_1 and C_2 and one projector P in a fix geometric arrangement (see fig. 2 right).

In the following the basic principles of fringe projection based 3D surface measurement should be briefly explained.

2.1 Phasogrammetry

Phasogrammetry is the connection of the mathematical principles of photogrammetry and fringe projection. The classical approach of fringe projection is described e.g. by Schreiber and Notni (Schreiber & Notni, 2000), which has been extended depending on several applications (Reich et al., 2000; Chen & Brown, 2000). The principle should be briefly explained as follows. A fringe projection unit projects one or two perpendicular, well defined fringe sequences onto the object, which is observed by one or more cameras. These

sequences may consist of a binary code sequence as the Gray code (Sansoni et al., 1999; Thesing, 2000) and a sequence of up to 16 sinusoidal fringe patterns. The so called rough phase value (Schreiber & Notni, 2000), and in combination with the Gray code the unique unwrapped phase value (Sansoni et al., 1999) is obtained using the sequence of sinusoidal patterns. Unique phase values are used to realize point correspondences in order to obtain measurement values by triangulation (Luhmann et al., 2006).

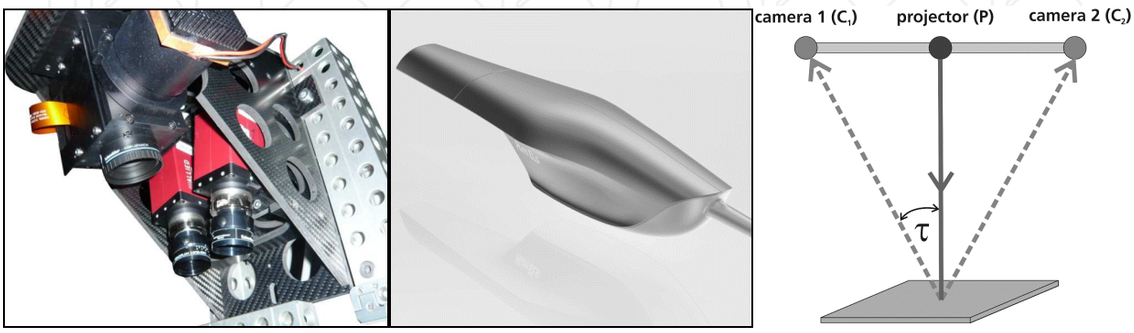


Fig. 2. High speed sensor HS (left), intraoral sensor DirectScan (middle), and typical sensor arrangement (right)

The rough phase value is the phase position within one period and the unique phase value is obtained by phase unwrapping leading to a monotone series of phase values (if error free) in a certain direction.

Phase values are produced in order to identify projector image coordinates or to produce virtual landmarks (Kühmstedt et al., 2007). These markers may be used both for calibration of the system and for the calculation of the 3D measurement data.

One sequence of fringe images is processed resulting in phase images $\Phi_{i,x}$ for each measuring position and each camera C_i. After rotation of the fringe pattern by 90°, the sequence may be projected and observed again resulting in a second phase image $\Phi_{i,y}$ for each camera. The phase values $\phi_{i,x}$ and $\phi_{i,y}$ (see fig. 3) correspond to image coordinates in the projector plane. The resulting 3D points are obtained by triangulation between the coordinates of the camera and the projector, or between corresponding points of two cameras. This can be regarded as standard procedure in photogrammetry (Luhmann et al., 2006).

2.2 Stereo vision and epipolar geometry

Using active stereo vision, images of the object are captured from two different perspectives. Pairs of image coordinates resulting from the same object point (the homologous points) have to be identified. The object can be reconstructed by triangulation using these points. In the case of active stereo vision a single intensity pattern or a sequence of patterns is projected onto the measurement object. There are several techniques to identify the homologous points in both cameras as e.g. described by Luhmann (Luhmann et al., 2006).

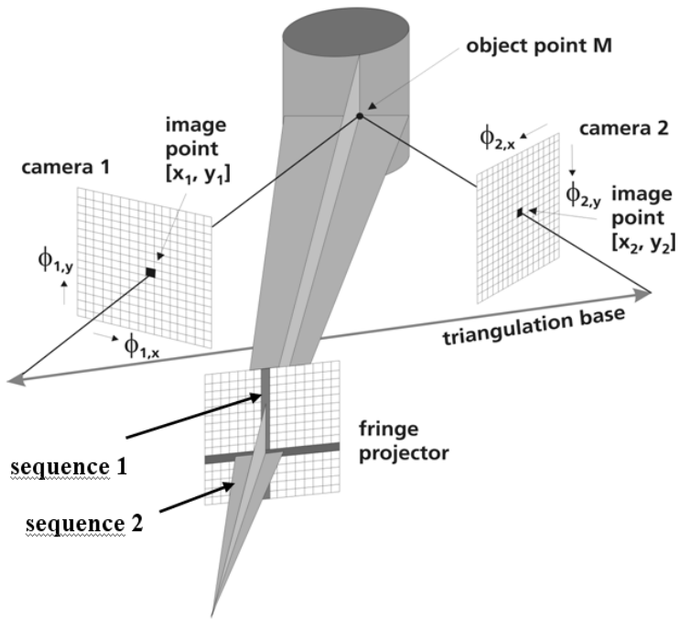


Fig. 3. Principle of phasogrammetry

Epipolar geometry is a well-known principle which is often used in computer vision when stereo systems are present. It is characterized by an arrangement of two cameras observing almost the same object scene. The projection centres O_1 and O_2 of the two cameras define together with an object point M a plane E in the 3D space (see fig. 4). The images of E are corresponding epipolar lines concerning M. When the image point m_1 of M is selected in the image I_1 of camera C_1, the corresponding point m_2 in the image I_2 of camera C_2 must lie on the corresponding epipolar line. This restricts the search area in the task of finding corresponding points. In the following we assume a system consisting of two cameras C_1 and C_2 and one projector P in a fixed arrangement.

Epipolar constraint usage is advantageous compared to using second fringe projection direction because only 50% of the recorded images are necessary. However, the calibration should be accurate and stable because correspondence finding is performed only on a line. Systematic errors of the sensor geometry lead to systematic errors of the position determination of the corresponding point to be found (Bräuer-Burchardt et al., 2011c).

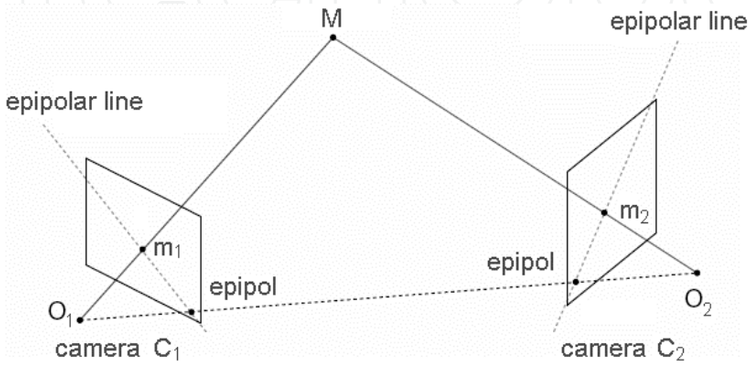


Fig. 4. Epipolar geometry

2.3 Camera calibration

Camera calibration describes the process of the determination of the intrinsic and extrinsic parameters (including lens distortion parameters) of an optical system. It has been extensively described in the literature, e.g. in (Brown, 1971; Tsai, 1986; Chen and Brown, 2000; Luhmann et al., 2006). Different principles have been applied in order to conduct camera calibration. The choice of the method depends on the kind of the optical system, the exterior conditions, and the desired measurement quality. In case of the calibration of photogrammetric stereo camera pairs, the intrinsic parameters (principal length, principal point, and distortion description) of both cameras should be determined as well as the relative orientation between the cameras.

The position of the camera in the 3D coordinate system is described by the position of the projection centre O = (X, Y, Z) and a rotation matrix R obtained from the three orientation angles ω, ϕ, and κ. Considering stereo camera systems, only the relative orientation between the two cameras (Luhmann et al., 2006) is considered, because the absolute position of the stereo sensor is usually out of interest.

Lens distortion may be considerable and should be corrected by a distortion correction operator D. It can be described by distortion functions or by a field of selected distortion vectors (distortion matrix). The determination of D is performed within the calibration procedure (Tsai, 1986) or separately (Bräuer-Burchardt, 2004).

3. Different concepts of accurate point correspondence determination

Correspondence determination in a stereo system means first the identification and, second, the localization of the point coordinates in the two considered 2D images mapping the same original 3D point.

The first task can be solved using a suitable method which depends on the actual conditions of the measurement. As phase values are concerned as the basis of the point correspondence finding we distinguish between methods producing unique phase values (e.g. using Gray code sequences or multi frequency projection techniques) and periodically repeating rough phase values.

In this work we assume to use a technique leading to unique phase values either in one or two directions. How to obtain unique phase values can be read elsewhere e.g. in (Battle et al., 1998; Zhang et al., 1999; Sansoni et al., 1999; Li et al., 2005; Bräuer-Burchardt et al., 2011a). Assume in the following that the uniqueness problem is solved.

In this section different concepts of correct point localization should be considered. These concepts distinguish e.g. concerning the hardware effort (one or two cameras), the costs, and the error sensitivity.

3.1 The CP method

The CP method is the simplest method to localize point correspondences and realize 3D point calculation.

Finding point correspondences is performed as follows. The pixels of camera C_1 are the coordinates x_1, y_1 of a point $p_1 = (x_1, y_1)$ and the observed phase values (ξ and η) at p_1

determine the coordinates of the corresponding point in the projector image plane. Together with the intrinsic camera parameters of C_1 and P and the relative orientation between C_1 and P, the 3D point is calculated by triangulation (see fig. 3).

For this method only one camera is used and no algorithmic effort for finding corresponding points is necessary. Hence this is also the simplest method concerning the computational effort. Additionally, because only two major hardware sensor components (one camera and one projector) are necessary, such sensors become lightweight and cheap. These aspects are advantageous whereas the dispensation with the second camera may be unfavourable. Figure 5 (left) shows a sketch of the CP arrangement.

The random error of the 3D point measurement is determined by the uncertainty of the phase determination and its scaling depends on the triangulation angle (see section 5).

3.1.1 CP algorithm

Precondition: Projection and observation (by one camera C_1) of a fringe image series consisting of two 90° rotated sequences subsequently producing two phase images Φ_x and Φ_y (*)

Input: two phase images Φ_x and Φ_y (*) for the observation camera C_1

Consider all pixels of the image I_1 of camera C_1. Let $p_i=(x_i, y_i)$ the coordinates of point p_i.

- Read the phase values ξ_i and η_i at p_i: $q_i =(\xi_i, \eta_i)$
- Perform triangulation between p_i and q_i to obtain 3D point P_i

Output: point cloud $\{P_i\}$

(*) Remark: The CP algorithm works also using only one projected fringe direction. Then, triangulation is performed between a ray and a plane in the 3D space.

3.2 The CPE method

The CPE method is the simple extension of the CP mode according to epipolar geometry. The second projected fringe direction is omitted. Instead of it the geometric information of the epipolar lines is used. The second coordinate of the observed phase value results from the position of the epipolar line in the projector image plane as illustrated by fig. 5 (right).

The advantages of the CPE method are the same as those of CP together with a reduced image sequence (half the number of images) meaning shorter projection and observation time and subsequently leading to shorter measurement time. Additionally, calculation time is reduced, too. The disadvantage is a reduced robustness of the coordinate determination, mainly determined by the epipolar lines. This can be, however, prevented by additional control measurements as e.g. suggested by the authors (Bräuer-Burchardt et al., 2011c).

3.2.1 CPE algorithm

Precondition: Projection of a fringe image series in one direction subsequently producing one phase image Φ_x and observation (by one camera C_1)

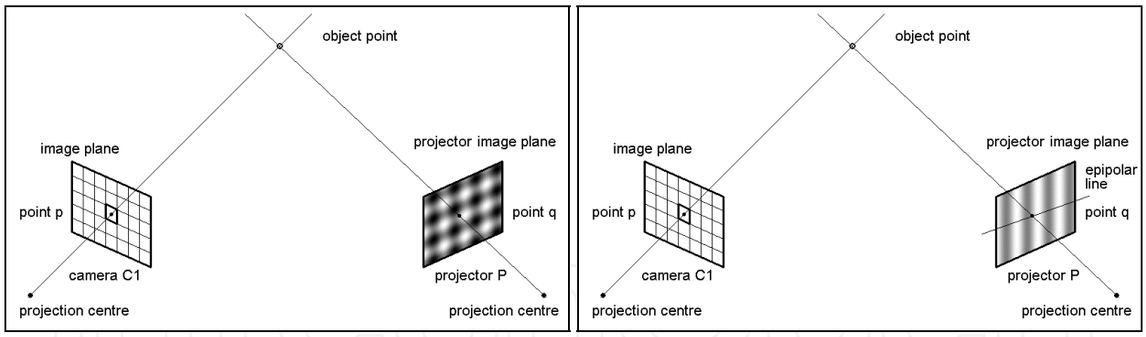


Fig. 5. Projector and camera arrangement for the CP (left) and the CPE (right) algorithms

Input: one phase image Φ_x for the observation camera C_1

Consider all pixels of the image I_1 of camera C_1. Let $p_i=(x_i, y_i)$ the coordinates of point p_i.

- Calculate the epipolar line g_i in the projector image plane corresponding to p_i
- Read the phase value ξ_i at p_i:
- Find the position $q_i =(\xi_i, \eta_i)$ of phase value ξ_i on g_i
- Perform triangulation between p_i and q_i to obtain 3D point P_i

Output: point cloud $\{P_i\}$

3.3 The CC method

The CC method (see Munkelt et al., 2005; Kühmstedt et al., 2007) uses corresponding points in the images of the two cameras C_1 and C_2 (see fig.1). For finding the point correspondence camera C_1 is disclaimed as primary camera. The camera pixels of C_1 are the coordinates of the point $p_1 = (x_1, y_1)$. The phase values $\phi = (\xi, \eta)$ at p_1 are searched for in the image of camera C_2. This search may use bilinear or bicubic interpolation and determines the exact position $p_2 = (x_2, y_2)$ of (ξ, η) with subpixel accuracy in the image of camera C_2 (see fig. 6). Together with the intrinsic camera parameters of C_1 and C_2 and the relative orientation between C_1 and C_2 the 3D point is calculated by triangulation.

The same procedure can be performed using C_2 as primary camera and determining the position of the corresponding point in the C_1 image with subpixel accuracy.

The main advantage of the CC technique over the CP method is the possibility to correct errors influenced by disturbed illumination or characteristic line errors. If the illumination is disturbed in both images in the same manner the error is similar and the correspondence will be found correctly despite the disturbance. This effect was reported by Munkelt (Munkelt et al., 2005).

The main disadvantage is the additional camera leading to higher weight and bigger volume of the sensor, higher costs, and an increased calculation effort.

3.3.1 CC algorithm

Precondition: Projection and observation (by two cameras C_1 and C_2) of a fringe image series consisting of two 90° rotated sequences subsequently producing two phase images Φ_x and Φ_y for each camera

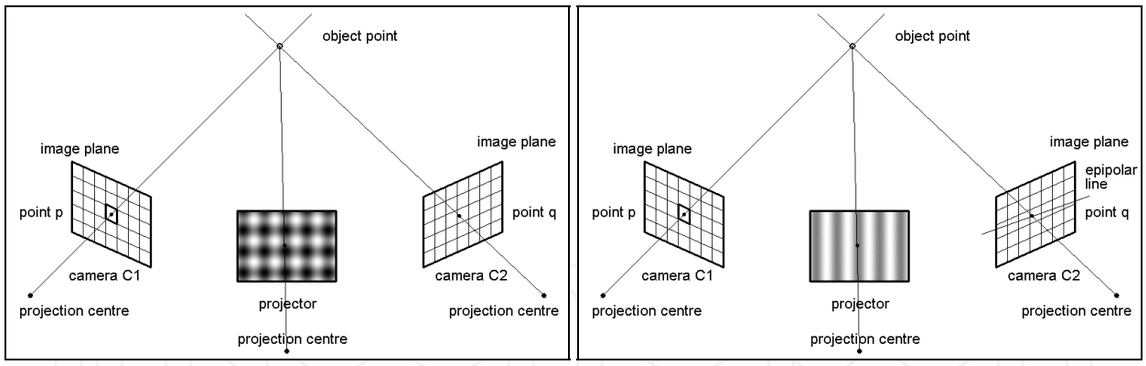


Fig. 6. Sensor arrangements for the CC (left) and the CCE (right) algorithms

Input: four phase images Φ_{1x}, Φ_{1y}, Φ_{2x} and Φ_{2y} for both observation cameras C_1 and C_2

Consider all pixels of the image I_1 of camera C_1. Let $p_i=(x_i, y_i)$ the coordinates of point p_i.

- Read the phase values ξ_i and η_i at p_i: $\phi_i = (\xi_i, \eta_i)$, i=1,2
- Find coordinates $q_i=(u_i, v_i)$ in the image of C_2 with phase values $\phi_i = (\xi_i, \eta_i)$
- Perform triangulation between p_i and q_i to obtain 3D point P_i

Output: point cloud $\{P_i\}$

3.4 The CCE method

The CPE method is the extension of the CP mode according to epipolar geometry. Instead of the second projected fringe direction the geometric information of the epipolar lines in the image I_2 of camera C_2 concerning the considered image point coordinates p=(x, y) are used.

The advantage of the method is the connection of the advantages of the CC method together with the epipolar constraint use. The disadvantages are analogous.

3.4.1 CCE algorithm

Precondition: Projection of a fringe image series in one direction subsequently producing one phase image Φ_{1x} and Φ_{2x} for each of the two cameras C_1 and C_2

Input: phase images Φ_{1x} and Φ_{2x} for the observation cameras C_1 and C_2

Consider all pixels of the image I_1 of camera C_1. Let $p_i=(x_i, y_i)$ the coordinates of point p_i.

- Calculate the epipolar line g_i in image I_2 of camera C_2 corresponding to p_i
- Read the phase value ξ_i at p_i:
- Find the position $q_i = (\xi_i, \eta_i)$ of phase value ξ_i on g_i
- Perform triangulation between p_i and q_i to obtain 3D point P_i

Output: point cloud $\{P_i\}$

3.5 The VR method

The VR method (VR means virtual raster) is derived from the CC method. Instead of taking the measured phase values at the pixels of one of the two cameras, a virtual phase raster is

defined according to the desired 3D point density in the resulting point cloud. The position of every phase raster point is determined in the image of the C_1 camera as well as in the image of the C_2 camera (see fig.2, right). If both positions $p_1 = (x_1, y_1)$ and $p_2 = (x_2, y_2)$ are detectable, the triangulation can be performed and the resulting 3D point can be calculated.

The advantage of the VR method is the possibility to choose an arbitrary spatial resolution of the resulting 3D measurement data. However, it should be noticed that neighbouring resulting points may be not independent. Here a particular careful error analysis based e.g. on the work of Notni (Notni & Notni, 2003) should be performed.

3.5.1 VR algorithm

Precondition: Projection and observation (by two cameras C_1 and C_2) of a fringe image series consisting of two orthogonal sequences subsequently producing two phase images Φ_x and Φ_y for both cameras C_1 and C_2

Input: four phase images Φ_{1x}, Φ_{1y}, Φ_{2x} and Φ_{2y} for both observation cameras C_1 and C_2

Consider all phase values $\phi_i = (\xi_i, \eta_i)$ of the selected raster.

- Find coordinates $p_i=(x_i, y_i)$ with the phase values $\phi_i = (\xi_i, \eta_i)$ in C_1
- Find coordinates $q_i=(u_i, v_i)$ with the phase values $\phi_i = (\xi_i, \eta_i)$ in C_2
- Perform triangulation between p_i and q_i to obtain 3D point P_i

Output: point cloud $\{P_i\}$

3.6 The VRE method

The VRE method is obtained by extension of the VR method by epipolar constraint. It can be achieved by fixing the raster of the searched phase values. However, the raster of the selected epipolar lines must be fixed, too. Usually the raster step width must be different because one direction is driven by the phase and the other by a metric default value.

Hence it is doubtful whether the usage of the VRE method would be meaningful. Too few experiments have been performed yet. A really convincing contention could only be given, if further analysis and experiments would have been successfully performed.

3.6.1 VRE algorithm

Precondition: Projection of a fringe image series in one direction subsequently producing one phase image Φ_x for each camera C_1 and C_2

Input: two phase images Φ_{1x} and Φ_{2x} for the observation cameras C_1 and C_2

Predefine a bundle of corresponding epipolar lines $g_{i,1}$ and $g_{i,2}$ in both camera images

Consider all phase values ξ_i of the selected raster

- Find coordinates $p_i=(x_i, y_i)$ with the phase value ξ_i on $g_{i,1}$
- Find coordinates $q_i=(u_i, v_i)$ with the phase value ξ_i on $g_{i,2}$
- Perform triangulation between p_i and q_i to obtain 3D point P_i

Output: point cloud $\{P_i\}$

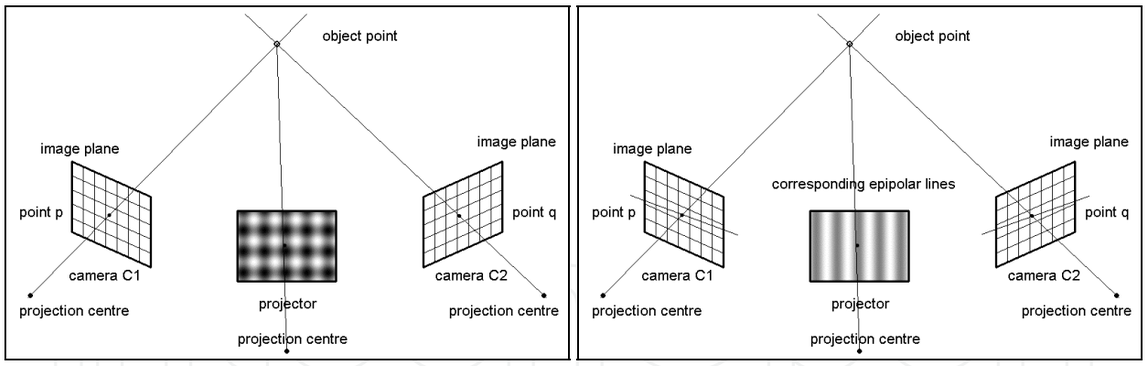


Fig. 7. Sensor arrangements for the VR (left) and the VRE (right) algorithms

4. Random and systematic errors at point correspondence localization

In order to evaluate and to compare all the different correspondence finding methods, an estimation of the error of the reconstructed 3D points was performed. The 3D error of a reconstructed point depends on a number of influences including phase measurement error, characteristic line error, calibration error, distortion, and others, having a systematic and a random component. All error sources that are not depending on the correspondence algorithm are assumed to have the same influence on the measurement accuracy of all considered methods.

Assuming that the determined calibration is fixed and the error of the calibration occurs as a systematic error, the phase noise has the main influence on the random error of the resulting 3D point. All other relevant error sources are expected to be systematic and are not considered here. A detailed analysis of the phase error is described by Notni (Notni & Notni, 2003).

4.1 Error models

As suggested by Rivera-Rios (Rivera-Rios et al. 2000) we assume a Gaussian independent random error $\Delta p=(\Delta x, \Delta y)$ of the observed point coordinates in the camera images. This leads to a certain random error $\Delta P=(\Delta X, \Delta Y, \Delta Z)$ of the measured 3D coordinate of the reconstructed point, additionally depending on the triangulation angle τ. This error is not symmetric in X, Y, and Z. The smaller the triangulation angle the higher is the longitudinal error compared to the lateral one. The amount of the error in the different coordinates depends on the orientation of the cameras in the world coordinate system W, too.

Assume the orientation of the world coordinate system with Z-axis along the boresight of the sensor obtained by a transform of W yielding W'. Then the standard deviations in X-, Y- and Z-direction of the measured point cloud characterize the lateral and longitudinal aspects of the random error of the measurement.

However, in the case of our correspondence methods CP and CC the point clouds characterizing the error of one measured point are deformed to a flat (situated nearly in a plane) point cloud. This is because one coordinate (the phase value or one camera pixel) is fixed. In the case of VR the shape of the error point cloud is the intersection of two cones (see fig. 9).

The extensions to CPE, CCE, and VRE by epipolar constraint reduce the shape of the error clouds again: to a line segment in the CPE and CCE case and to a flat ellipse in the VRE case (see figs. 8 and 9). Initially, this means a reduction of the random error by use of epipolar constraint. However, a systematic error may additionally occur in the case of a calibration error. This error, however, may be reduced by some additional effort as shown by the authors (Bräuer-Burchardt et al., 2011c).

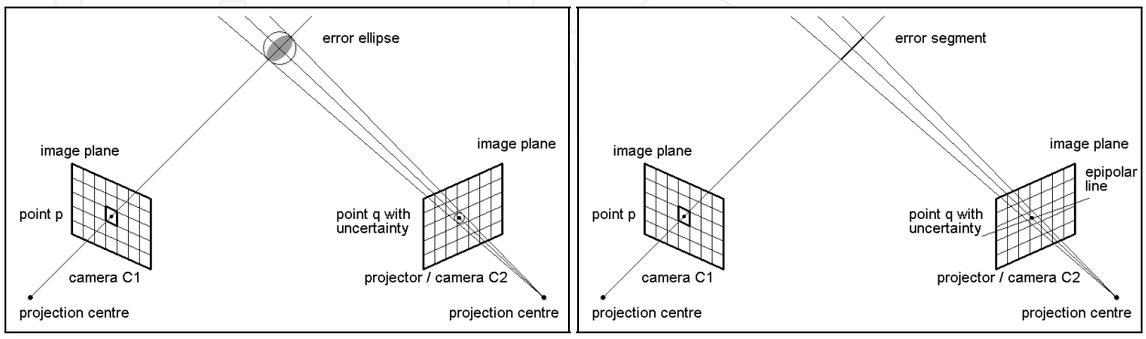


Fig. 8. Error model for CP/CC (left) and CPE/CCE (right)

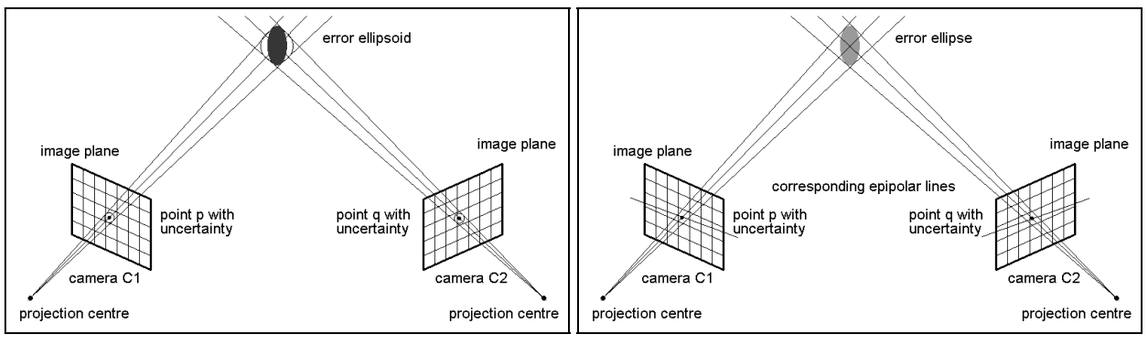


Fig. 9. Error model for the VR (left) and the VRE (right) algorithms

In order to estimate the random error of a single point measurement the following assumptions are made. Assume that the calibration is fix and error free, and a possible distortion error is completely corrected. The error Δp of the camera coordinate of a certain point representing a given phase value should be normally distributed with expectation value $E(\Delta p)=0$ and a certain variance $\sigma_c^2(\Delta p)$ which should be equal in X- and Y- direction. The amount of this error depends on the phase noise (depending on the measuring conditions, number of images in the sequence (Notni & Notni, 2003), and the parameters of the current filter operators (e.g. Gaussian).

Let σ_c be the standard variation of the random error of the pixel coordinate after all filtering operations, m the magnification of the mapping and M the inverse magnification M=1/m.

Let us consider first the case CP/CC and the transformed world coordinate system W'. Because of the fixed coordinate in the primary camera, the random error of the measured 3D point depends only on the random error in one camera image and the triangulation angle τ. We consider the standard deviations $\sigma_x(\Delta p)$, $\sigma_y(\Delta p)$, and $\sigma_z(\Delta p)$ of the calculated 3D point coordinates. We obtain

$$\sigma_x \approx 0; \quad \sigma_y \approx \frac{1}{2}\sigma_c \cdot M \cdot fac; \quad \sigma_z \approx \frac{1}{\sin(\tau)}\sigma_c \cdot M \cdot fac \tag{1}$$

where *fac* is set to *fac* = 1 for both the CP and the CC mode. Rather it should be *fac* = 1 for CP and $fac = \sqrt{2}$ for the CC method because of the double uncertainty of the phase value. However, a number of experiments showed that the random error of CC is equal to that of CP mode using the same triangulation angle. We assume that usually some error sources have the same influence to the phase error in both images of cameras and hence this causes the reduction of $fac = \sqrt{2}$ to *fac* = 1 also in the CC mode.

Considering CPE and CCE we obtain

$$\sigma_x \approx 0; \quad \sigma_y \approx 0; \quad \sigma_z \approx \frac{1}{\sin(\tau)}\sigma_c \cdot M \cdot fac \tag{2}$$

for both the CPE and the CCE mode.

Considering VR and assuming an independent random error Δp with E(Δp)=0 and $\sigma_c^2(\Delta p)$ of the same amount in the two camera images, we obtain

$$. \sigma_x = \frac{1}{\sqrt{2}}\sigma_c \cdot M; \quad \sigma_y = \frac{1}{\sqrt{2}}\sigma_c \cdot M; \quad \sigma_z = \frac{\sqrt{2}}{\sin(\tau)}\sigma_c \cdot M \tag{3}$$

and for VRE we get

$$. \sigma_x \approx 0; \quad \sigma_y \approx 0; \quad \sigma_z = \frac{\sqrt{2}}{\sin(\tau)}\sigma_c \cdot M \tag{4}$$

As we can see considering formulas (1) to (4) CPE and CCE provide the best estimation of the random 3D error because the error only depends on the uncertainty of the phase determination along the epipolar line. However, an additional systematic error can occur due to the uncertainty of the epipolar line position. It may be erroneous due to calibration errors caused by thermic or mechanic influences as shocks or vibrations. However, the stability of the calibration can be checked, and hence this error can be estimated and minimized as it was shown by the authors (Bräuer-Burchardt et al., 2011c). CP/CC and CPE/CCE errors are mainly influenced by the triangulation angle τ.

5. Experiments and results

5.1 Simulations

In order to estimate the random error of a 3D point measurement and to confirm the theoretic assumptions according to formulas (1) and (2), the following simulation experiment was performed. For a given geometric situation of the sensor (extrinsic and intrinsic parameters of the camera(s) and the projector, triangulation angle between the two relevant image normal vectors) a meaningful value of the random error Δp of the camera coordinates was chosen. It was chosen a normally distributed random value Δp = (Δx, Δy) with expectation value (0, 0) for the camera coordinate uncertainty. The variance was chosen

according to realistic conditions by experiment. The error ΔE of the calculated 3D point coordinate is given as (ΔX, ΔY, ΔZ) error vector in the virtual world coordinate system W'. The alignment of W' is according to the orientation of the boresight of the contributing cameras (C and P or C_1 and C_2, resp.).

Error estimation will be achieved by analysis of the covariance matrix of the coordinate values of the point clouds. These point clouds are those of the measured or simulated points in the world coordinate system W according to the calibration data. The variances of the error vector components are obtained as the eigenvalues ev_1, ev_2, and ev_3 of the covariance matrix. Hence the random error of the 3D point calculation can be described by the standard deviations in the virtual world coordinate system W' corresponding to the square roots of the eigenvalues:

$$ls_x = \sqrt{ev_1}; \quad ls_y = \sqrt{ev_2}; \quad ls_z = \sqrt{ev_3} \tag{5}$$

The simulation of a measurement with random error was performed 400 times. The resulting 3D point cloud was analysed using covariance matrix leading to the 3D point error characteristic (σ_x, σ_y, and σ_z). For the VR case the image coordinate of the pixels of camera C_1 were disturbed by a 2D error value with the same statistical characteristics (normal distribution, zero expectation value, same variance as for C_2), too.

The standard deviations of the three coordinates in the transformed world coordinate system W' according to (1) and (2) and the simulation results using 400 measurements are given in table 1 showing that it holds approximately $\sigma_x = ls_x$, $\sigma_y = ls_y$, and $\sigma_z = ls_z$.

exp. status	quantity \ mode	CP	CPE	CC	CCE	VR	VRE
	τ [°]	11,2	11,2	24,0	24,0	24,0	24,0
model	σ_x [µm]	0,0	0,0	0,0	0,0	1,6	1,6
	σ_y [µm]	1,2	0,0	1,2	0,0	1,6	0,0
	σ_z [µm]	11,9	11,9	5,7	5,7	8,0	8,0
simulation	ls_x [µm]	0,0	0,0	0,0	0,0	1,7	1,6
	ls_y [µm]	1,2	0,0	1,3	0,0	1,7	0,0
	ls_z [µm]	13,0	12,8	6,0	5,9	8,0	8,1
experiment	ls_x [µm]	0,003	0,003	0,003	0,003	1,0	1,0
	ls_y [µm]	1,1	0,003	1,0	0,003	1,2	0,005
	ls_z [µm]	11,0	11,0	6,0	6,0	9,4	9,4

Table 1. Model data, simulation data, and experimental data of measurements using different methods

5.2 Experiments on real measurements

In order to evaluate the different correspondence finding methods several experiments determining the accuracy of the measurements were performed. For the measurements the "kolibri flex mini" system was used. This system (see fig.1) is a table top system with a sensor head consisting of two cameras (1.4 Mpixels) and one projector. The working distance is about 300 mm and the measuring volume is 90 mm (diameter) x 25 mm (height).

The measuring accuracy given by the standard deviation of the surface points on a plane is about 5 µm.

The first experiment was a measurement of a single point in repeated measurements in order to confirm the simulation experiment described in the previous section. The number of measurements was 400. The resulting *ls*-values of all measurements are listed in table 1 and confirm the theoretic assumptions.

The next experiment was performed in order to confirm the assumption about the dependence of the random error on the triangulation angle. Different triangulation angles were realized by a modification of the "kolibri flex mini" system. Each measurement with one fix triangulation angle and using the VR mode was repeated at least 100 times. A range between 5 and 40° was realized for the triangulation angle τ.

The results of the variation of the triangulation angle are shown by a plot of the accuracy values in fig. 10.

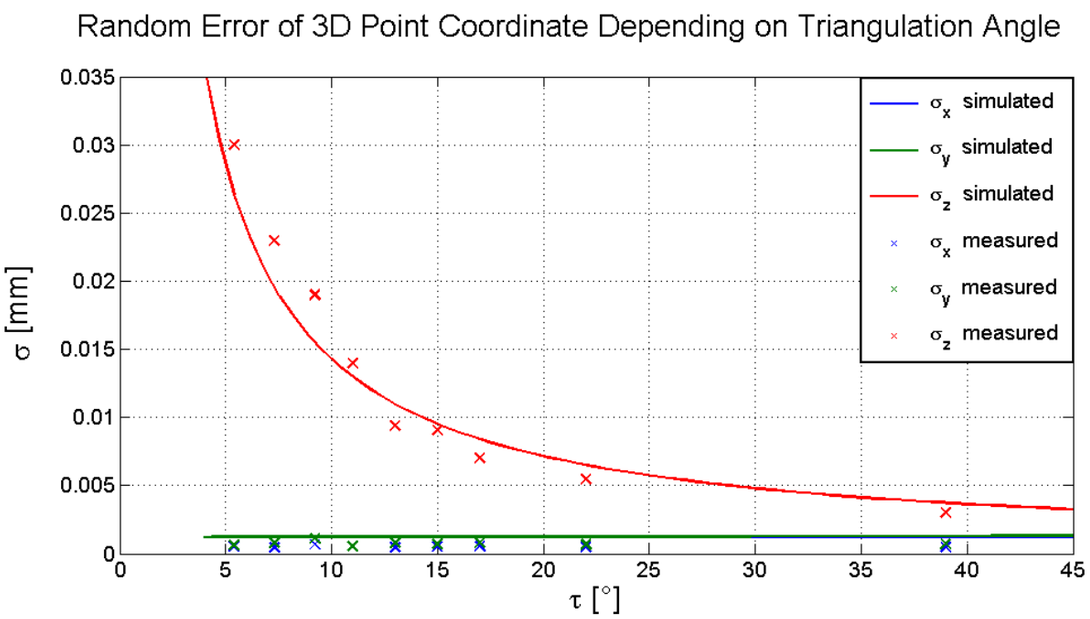


Fig. 10. Plot of accuracy of VR mode depending on triangulation angle τ

6. Discussion

The results of the experiments and the simulations mainly confirm the theoretic analysis of the measuring accuracy. Especially in the CP/CPE and CC/CCE modes the correlation between the results is very high. Using the VR/VRE modes, too few experiments have been performed in order to make significant statements. Here, additional effects may influence the random error and lead to a difference to our model. This will be, however, analysed in our future work.

The completeness of a measurement is directly dependent on the triangulation angle. The smaller the triangulation angle the bigger is the number of measured 3D points because shadowing and occlusion effects are reduced. Otherwise, if triangulation angle becomes too small, σ_z error increases. However, a difference of the completeness between a CP/CPE and

a CC/CCE measurement with $\tau_{CC} = 2\tau_{CP}$ also depends heavily on the shape of the measuring object.

In general, CP/CPE mode and CC/CCE mode with the same triangulation angle $\tau_{CC} = \tau_{CP}$ provide the same results in the accuracy. However, having disturbances in the phase generation which similarly occur in both camera images (e.g. by indirect illumination, irregular reflexes, phase generation errors, characteristic line errors, or not corrected distortion of the projector optics) the error using the CC/CCE mode may be considerable smaller than using CP/CPE mode as described by Munkelt (Munkelt et al., 2005).

The results are helpful for the decision of the method to be used taking into account the typical measuring objects, the demands on the measurement, and the costs already in the phase of system design.

A combination of the methods may improve a measurement using only one method concerning accuracy and/or completeness in certain cases depending on the measuring object as suggested by the authors (Bräuer-Burchardt et al., 2010). However, this requires additional algorithmic effort in the generation of software tools which has not been realized yet for our systems. It also extends the calculation time and will not be used in fast speed applications. However, first tests of the combination of the CP and VR methods have been successfully performed in order to obtain data of regions which were hidden or in the shade using only CC mode.

Together with the results described by Kühmstedt (Kühmstedt et al., 2009), a comprehensive prediction of the expected error of 3D measurement systems using fringe projection can be made depending on the properties of the measuring device, the exterior conditions and the measuring objects.

As already mentioned in section 3 the main advantage of the CP/CPE method is the minimal effort in equipment and calculation in contrast to the usage of the CC/CCE mode. There, however, illumination caused errors may be reduced by the principle (Munkelt et al., 2005).

The extension by use of the epipolar constraint is always meaningful because it saves half of the recording time and reduces the random error in direction perpendicular to the epipolar lines. However, it should be realized that the calibration is correct and stable which can be checked by additional measurements.

In order to design a new sensor the choice of the selected point localization principle depends on several aspects like requested measurement accuracy, field of application, measurement conditions (e.g. illumination, sensor mounting, measuring objects), costs, sensor weight, and so on. Hence, this work cannot give the optimal way to perfect measurement data but it may help to understand the influences on the measurement accuracy.

7. Summary and outlook

In this work some different correspondence localization methods which are usually applied in 3D measurement systems using fringe projection were compared concerning the measuring accuracy. A theoretic model for the random error of the measured 3D point coordinates was established. A simulation tool was developed and applied. The results obtained by these estimations were confirmed by real measurement data.

Future work is addressed on several aspects. First, the accuracy determination of the VR/VRE modes should be improved and the error model should be potentially extended. Here a number of new experiments must be performed.

Second, a combination of some of the methods should be merged into one measuring system in order to obtain more complete results in the case of difficult measuring object geometries. Here, new algorithms which realize an automatic 3D data fusion, a smooth passage between regions of different measuring uncertainties, and an optimization of the connected data must be developed.

Third, the VR/VRE methods can be extended in order to obtain equidistant distributed 3D points as result of a measurement. This involves the realization of an adaptive virtual phase raster for the point corresponding algorithms. Here, information about the shape of the measuring object is necessary that may be obtained in a preliminary rough measurement.

8. References

Battle J., Mouaddib, E. & Salvi, J. (1998). Recent progress in coded structured light as a technique to solve the correspondence problem: a survey. PR, Vol. 31, No 7, 963-982

Bräuer-Burchardt, C. (2004). A Simple New Method for Precise Lens Distortion Correction of Low Cost Camera Systems. Pattern Recognition (Proc 26th DAGM-Symposium), Springer, 570-77

Bräuer-Burchardt, C., Möller, M., Munkelt, C., Kühmstedt, P. & Notni, G. (2010). Comparison and evaluation of correspondence finding methods in 3D measurement systems using fringe projection. Proc. SPIE Vol. 7830, 783019-1 - 783019-9

Bräuer-Burchardt, C., Munkelt, C., Heinze, M., Kühmstedt, P. & Notni, G. (2011a). Using Geometric Constraints to Solve the Point Correspondence Problem in Fringe Projection Based 3D Measuring Systems. Proc. ICIAP 2011, Part II, Springer LNCS, 265-74

Bräuer-Burchardt, C., Breitbarth, A., Kühmstedt, P., Schmidt, I., Heinze, M. & Notni, G. (2011b). Fringe Projection Based High Speed 3D Sensor for Real-Time Measurements. Proc. SPIE, Vol. 8082, 808212-1 - 808212-8

Bräuer-Burchardt, C., Kühmstedt, P. & Notni, G. (2011c). Error compensation by sensor re-calibration in fringe projection based optical 3D stereo scanners. Proc. ICIAP 2011, Part II, Springer LNCS, 363 -73

Brown, D.C. (1971). Close-range camera calibration. Photogram. Eng. 37(8), 855-66

Chen, F. & Brown, G.M. (2000). Overview of three-dimensional shape measurement using optical methods. Opt. Eng. 39, 10-22

Creath, K. (1986). Comparison of phase-measurement algorithms. Surface characterization and testing. Proc. SPIE 680, 19–28

Ishiyama, R., Sakamotom, S., Tajima, J., Okatani, T. & Deguchi, K. (2007a). Absolute phase measurements using geometric constraints between multiple cameras and projectors. Applied Optics, Vol. 46, Issue 17, 3528-3538

Ishiyama, R., Okatani, T. & Deguchi, K. (2007b). Precise 3-d measurement using uncalibrated pattern projection. Proc. IEEE Int. Conf. on Image Proc., vol. 1, 225-228

Kühmstedt, P., Heinze, M., Himmelreich, M., Bräuer-Burchardt, C. & Notni, G. (2005). Optical 3D sensor for large objects in industrial application. Proc. SPIE 5856, 118-127

Kühmstedt, P., Munkelt, C., Heinze, M., Himmelreich, M., Bräuer-Burchardt, C. & Notni, G. (2007). 3D shape measurement with phase correlation based fringe projection. Proc. SPIE vol. 6616, 66160 B-1-B-9

Kühmstedt, P., Bräuer-Burchardt, C., Munkelt, C., Heinze, M., Schmidt, I., Hintersehr, J., Notni, G. (2007b). Intraoral 3D scanner. Proc. SPIE vol. 6762, 67620 E-1-E-9

Kühmstedt, P., Bräuer-Burchardt, C. & Notni, G. (2009). Measurement Accuracy of Fringe Projection Depending on Surface Normal Direction. Proc. SPIE vol. 7432, 743203,1-9

Li, E.B., Peng, X., Xi, J., Chicaro, J.F., Yao, J.Q. & Zhang, D.W. (2005). Multi-frequency and multiple phase-shift sinusoidal fringe projection for 3D profilometry. Optics Express. 13, 1561-1569

Li, Z., Shi, Y. & Wang, C. (2009). Real-time complex object 3D measurement. Proc. ICCMS, 191-194

Luhmann, T., Robson, S., Kyle, S. & Harley, I. (2006). Close range photogrammetry. Wiley Whittles Publishing

Maas, H.-G. (1992). Robust automatic surface reconstruction with structured light. IAPRS, Vol. XXIX, Part B5, 709-713

Munkelt, C., Kühmstedt, P., Heinze, M., Süße, H. & Notni, G. (2005). How to detect object-caused illumination effects in 3D fringe projection. Proc. SPIE vol. 5856, 632-639

Notni, G. H. & Notni, G. (2003). Digital fringe projection in 3D shape measurement – an error analysis. Proc SPIE 5144, 372-80

Reich, C., Ritter, R. & Thesing, J. (2000). 3-D shape measurement of complex objects by combining photogrammetry and fringe projection. Opt. Eng. 39, 224–231

Rivera-Rios, A.H. & Marefat, M. (2005). Stereo Camera Pose Determination with Error Reduction and Tolerance Satisfaction for Dimensional Measurements. Proc. IEEE Int Conf on Robotics and Automation, 423-428

Sansoni, G., Carocci, M. & Rodella, R. (1999). Three-dimensional vision based on a combination of Gray-code and phase-shift light projection: Analysis and compensation of the systematic errors. Applied Optics, Vol. 38, Issue 31, pp. 6565-6573

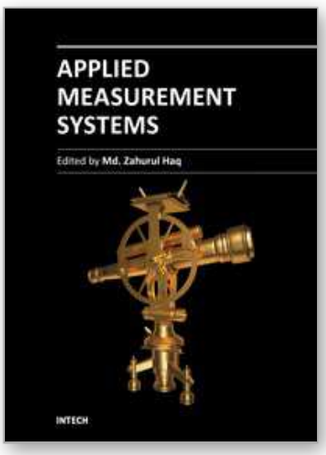
Schreiber, W. & Notni, G. (2000). Theory and arrangements of self-calibrating whole-body three-dimensional measurement systems using fringe projection techniques. Opt. Eng. 39, 159-169

Tsai, R. (1986). An efficient and accurate camera calibration technique for 3-D machine vision. IEEE Proc CCVPR, 364-74

Young, M., Beeson, E., Davis, J., Rusinkiewicz, S. & Ramamoorthi, R. (2007) Viewpoint-coded structured light. Proc. CVPR, 1-8

Zhang, H., Lalor, M.J. & Burton, D.R. (1999). Spatiotemporal phase unwrapping for the measurement of discontinuous objects in dynamic fringe-projection phase-shifting profilometry. Applied Optics. 38, 3534-3541

Zhang, S. & Yau, S.T. (2006). High-resolution, real-time 3D absolute coordinate measurement based on a phase-shifting method. Optics Express, Vol. 14, Issue 7, 2644-2649



Applied Measurement Systems

Edited by Prof. Zahurul Haq

ISBN 978-953-51-0103-1
Hard cover, 390 pages
Publisher InTech
Published online 24, February, 2012
Published in print edition February, 2012

Measurement is a multidisciplinary experimental science. Measurement systems synergistically blend science, engineering and statistical methods to provide fundamental data for research, design and development, control of processes and operations, and facilitate safe and economic performance of systems. In recent years, measuring techniques have expanded rapidly and gained maturity, through extensive research activities and hardware advancements. With individual chapters authored by eminent professionals in their respective topics, Applied Measurement Systems attempts to provide a comprehensive presentation and in-depth guidance on some of the key applied and advanced topics in measurements for scientists, engineers and educators.

How to reference

In order to correctly reference this scholarly work, feel free to copy and paste the following:

Christian Bräuer-Burchardt, Max Möller, Christoph Munkelt, Matthias Heinze, Peter Kühmstedt and Gunther Notni (2012). Determining Exact Point Correspondences in 3D Measurement Systems Using Fringe Projection – Concepts, Algorithms and Accuracy Determination, Applied Measurement Systems, Prof. Zahurul Haq (Ed.), ISBN: 978-953-51-0103-1, InTech, Available from: http://www.intechopen.com/books/applied-measurement-systems/determining-exact-point-correspondences-in-3d-measurement-systems-using-fringe-projection-concepts-a

INTECH
open science | open minds

InTech Europe
University Campus STeP Ri
Slavka Krautzeka 83/A
51000 Rijeka, Croatia
Phone: +385 (51) 770 447
Fax: +385 (51) 686 166
www.intechopen.com

InTech China
Unit 405, Office Block, Hotel Equatorial Shanghai
No.65, Yan An Road (West), Shanghai, 200040, China
中国上海市延安西路65号上海国际贵都大饭店办公楼405单元
Phone: +86-21-62489820
Fax: +86-21-62489821

© 2012 The Author(s). Licensee IntechOpen. This is an open access article distributed under the terms of the Creative Commons Attribution 3.0 License, which permits unrestricted use, distribution, and reproduction in any medium, provided the original work is properly cited.

IntechOpen

IntechOpen